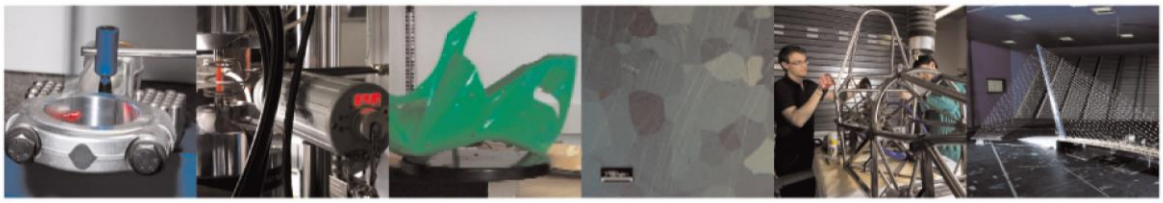

Laser micropolishing of AISI 304 stainless steel surfaces for cleanability and bacteria removal capability

De Giorgi, Chiara; Furlan, Valentina; Demir, Ali Gökhan; Tallarita, Elena; Candiani, Gabriele; Previtali, Barbara

This is a post-peer-review, pre-copyedit version of an article published in APPLIED SURFACE SCIENCE. The final authenticated version is available online at:
http://dx.doi.org/10.1016/j.apsusc.2017.02.083

DIPARTIMENTO DI MECCANICA ■ POLITECNICO DI MILANO
via G. La Masa, 1 ■ 20156 Milano ■ EMAIL (PEC): pecmecc@cert.polimi.it
http://www.mecc.polimi.it
Rev. 0

Laser micropolishing of AISI 304 stainless steel surfaces for cleanability and bacteria removal capability

Chiara De Giorgi[a*] chiara.degiorgi@mail.polimi.it, Valentina Furlan[a], Ali Gökhan Demir[a], Elena Tallarita[b], Gabriele Candiani[b], Barbara Previtali[a]

[a]Department of Mechanical Engineering, Politecnico di Milano, Via La Masa 1, 20156 Milan, Italy

[b]Department of Chemistry, Materials, and Chemical Engineering "Giulio Natta", Politecnico di Milano, Via Mancinelli 7, 20131 Milan, Italy

[*] Corresponding author. Tel.: +39 02 2399 8530; fax: +39 02 2399 8593.

Graphical abstract

Abstract

In this work, laser micropolishing (LμP) was employed to reduce surface roughness and waviness of AISI 304 stainless steel surfaces. A pulsed fibre laser operating in the ns regime was used and the influence of laser parameters in N_2-controlled atmospheres was evaluated. The surface remelting allowed to reduce the surface roughness by closing cracks and defects formed during the rolling process. Other conditions that did not improve the surface quality were analysed for defect typology. Moreover, laser treatments allowed the production of more hydrophobic surfaces, although no surface chemistry modification was identified. Surface cleanability were investigated on *Escherichia coli* (*E. coli*), evaluating the number of residual bacteria adhering to the substrate after a washing procedure. These results showed that LμP is a suitable way to lower the average surface roughness by about 60% and average surface waviness by approximately 36%. Besides, the surfaces treated with the optimized parameters of laser polishing process display a reduced amount of contaminant particle sticking on surfaces as compared to untreated surfaces.

Keywords: Laser micropolishing, antibacterial surface, antifouling, bacteria repelling, surface functionalization

1. Introduction

Surface cleanability is a critical aspect in a wide variety of scenarios ranging from surgical tools and water filtration, to ship hulls and food industry. Just the latter one provides a variety of conditions, such as the presence of moisture, nutrients and microorganisms from raw materials, which might favour surface and food contamination. In particular, the tendency of bacteria to adhere and colonize solid surfaces is one of the most potential source of contamination of food that may lead to the transmission of foodborne pathogens and the reduction in shelf-life. For these reasons, the main requirement for equipment used in these working divisions is the easy cleanability for the removal of bacteria and any other possible contaminant. The cleanability aspect refers to the efficacy of a fixed cleaning procedure with a given underlying surface as the surface can help to reduce bacterial adhesion without necessarily killing the bacteria. Indeed, the design of surfaces, that prevent bacterial fouling by means of their physical structure, represents a key area of research. Bacterial adhesion is a very complex process that is influenced by several factors [1], including the chemical and physical nature of the surface.

As several studies reported how polished surfaces and highly rough surfaces may prevent bacterial adhesion, it could be speculated that surface morphology significantly affects bacterial adhesion and moreover the bacteria removal capability [2]–[7]. In particular, it seems that bacterial attachment ability is enhanced when surfaces display dimensions similar to bacterial size [8]. This phenomenon may occur for three main reasons: *a)* presence of a higher surface area available for attachment; *b)* protection from shear forces; *c)* chemical modifications that cause preferential physicochemical interactions [9].

Another parameter that has to be taken into account is the surface wettability. Some studies reported that bacteria like *Staphylococcus aureus* (*S. aureus*) and *Escherichia coli* (*E. coli*) are more attracted by hydrophilic surfaces, whereas *Pseudoxanthomas taiwanensis* and *Staphylococcus epidermidis* display preferential adhesion on hydrophobic surfaces [9].

Given that the surface finishing plays a role in regulating the interaction with bacteria, a polishing treatment could be advisable to prevent bacterial adhesion enhancing surface cleanability through the control of both surface morphology (i.e. roughness) and its physio-chemical properties (i.e. wettability). Some polishing technologies can be successfully applied to obtain surface finishes in the nanometer range, such as abrasive polishing, lapping, mechano-chemical and ultrasonic polishing. Laser micropolishing (LμP) represents a valid and effective alternative to produce high levels of surface finish. LμP process basically consists in a remelting phenomenon: laser beam energy generates a melt pool on the workpiece surface, and the surface tension tends to redistribute the molten material around each initial surface asperity. Thus, after solidification, peak to valley heights, surface asperities as well as surface roughness are reduced [10].

LμP shows several major strengths, such as the possibility to treat a well-defined area with a full process automation and control. It is a single step process with no contact, excluding mechanical forces at tool-workpiece interface and tool wear. Conversely, the process of laser polishing displays also some drawbacks mainly because the process thermal, possibly generating a heat affected zone with different mechanical properties as compared to bulk material [10]–[12]. Moreover, it is strongly affected by the initial surface

topography and by the presence of surface defects that could vary the absorption or reflection of the incident radiation. Although several works report the suitability of LμP for highly polished surfaces, the achievement of low surface roughness, especially when the initial surface morphology has a quality, still remains one of the biggest challenges [10], [11], [13]–[15].

This work aims to understand the effect of surface finishing on the cleanability of stainless steel 304 alloy surface, that is a widely used material for different industrial purposes due to a combination of good mechanical properties and excellent corrosion resistance. In fact, this alloy is very often employed in environments and applications where antibacterial properties are required, such as in hospitals for surgical and dental instruments or for domestic tools industry and kitchen equipment. In particular, the process is aimed for food industry and kitchen environment, where this technique results an original and effective alternative to functionalized coatings. A fibre laser source in ns pulse regime was used to study the effect of process parameters on the surface roughness and waviness changes as well as on wettability and chemical composition. Among different conditions tested in a larger experimental campaign, the most promising surfaces were identified. They underwent cleanability analysis through bacteria adhesion experiments with a post-washing step. Such tests were carried out on *E. coli,* since it is one of the main causes of food contamination and foodborne illness [16].

2. Materials and methods

2.1. Material

Cold rolled 0.5 mm stainless steel 304 alloy sheets were used throughout the study. The surface average roughness Sa,r was 85±3 nm, while the surface average waviness Sa,w was 56±6 nm. Before LμP, the specimens were cleaned by means of an ultrasonic bath with deionized water (dH_2O, 10 min), ethanol (10 min) and dH_2O (10 min). Then the surfaces were dried under nitrogen (N_2). No further chemical or electrochemical treatments were applied. All chemicals and bacterial culture reagents were from Sigma Aldrich, if not differently specified.

2.2. Laser micropolishing setup

LμP was realized by a nanosecond pulsed fibre laser (YLP-1/100/50/50 from IPG Photonics, Oxford, MA, USA) emitting at 1,064 nm, coupled to a scanner head (TSH 8310 by Sunny Technology, Beijing, China). The scanner head included an f-theta lens (SL-1064-70-100 from Wavelength Opto-Electronic, Singapore), with 100 mm focal length. The workpiece was positioned inside a gas chamber to work under controlled atmosphere. During this work, N_2 was used as process gas to avoid oxidation during the process. Focal position was adjusted using a Z-axis with motorized lab jack from (L490MZ/M, from Thorlabs, Newton, NJ, USA). The main specifications of the employed laser system are summarized in Table 1.

2.3. Surface characterization

Scanning electron microscopy (SEM EVO-50, from Carl Zeiss, Oberkochen, Germany) images were acquired a qualitative analysis of the surface morphology. A focus variation microscopy (InfiniteFocus from Alicona Imaging GmbH, Graz, Austria) was employed for surface topography acquisitions and quantitative roughness/waviness measurements. Due to the high reflectivity of the polished surface, the focus variation microscopy was not appropriate to operate directly on stainless steel surfaces. Hence, the surfaces were replicated on silicon-based rubber (RepliSet by Struers, Ballerup, Denmark) and measured through the replicated rubber surfaces. The acquisitions were carried out at 100× objective, with estimated vertical resolution of 5 nm, and horizontal resolution of 90 nm. The acquisition area was 110.61×145.81 μm^2. Three areas were acquired on each surface. Average surface roughness (Sa) was calculated over each acquired area, applying a high-pass filter (for roughness profile Sa,r) and a low-pass filter (for waviness profile Sa,w) at a cut-off wavelength of 29.14 μm, according to the ASME B46.1-2002 [17].

Surface wettability was characterized through static contact angle measurement. Sessile drop technique was used employing 2 μL droplets of dH_2O.

The surface chemistry was investigated for candidate surfaces through energy-dispersive spectroscopy (EDS, Inca Energy 200 from Oxford Instruments, Abingdon, United Kingdom) and X-ray diffraction (XRD, PW1830 from Philips, Almelo, The Netherlands). EDS was employed to quantify the chemical composition down to 5 μm depth. XRD allowed for identifying the crystalline phases in the material for the first 10-20 μm deep from the surface.

2.4. Experimental plan

2.4.1. Laser micropolishing

The experimental campaign was designed around the feasibility window, which was determined in a previous work [18]. The used gas was N_2, since surface nitridation might positively influence the surface chemistry, as previously reported by others [19], [20]. Laser beam was focused 2 mm above the surface to generate 124 μm beam diameter (d_s) on the workpiece. In this way, the energy density can be lowered avoiding material ablation and providing surface remelting. LμP consisted of overlapping laser pulses on the material surface over scan lines and between adjacent scan lines. Laser pulse energy (E) was varied between 0.19 and 0.47 mJ. The overlapping on a single scan track depends on the beam diameter as well as pulse repetition rate (PRR) and scan speed (v). Pulse repetition rate was fixed at 65 kHz, whereas scan speed was varied between 12 and 192 m/min. The overlapping between adjacent scan lines was fixed with a pitch (p) at 10 μm. In order to investigate the effect of multiple passes over the same scanned area, three different scanning strategies were used with variable number of passes (N). Rolling direction was identified parallel to the longer axis of the coiled material. Moreover, the cold-rolled sheet material is characterised by a surface texture with elongated lines along the rolling direction, which was confirmed through optical microscopy and taken as the reference for scan angle (α). Single passes (N=1) were applied parallel to the rolling direction (α=0°). Scan angle was varied along with the number of passes, where for N=2 scan angle followed 0° and 90° and for N=4 scan angles were 0°, 90°, 45° and 135° (N=4). The experiments were conducted under N_2, setting the pressure inside the gas chamber constant at 0.3 bar. Different processing conditions were applied in patches of 3×3 mm^2. The complete experimental plan produced 60 different conditions. SEM images were taken for all the surfaces produced. Besides, surface roughness (Sa,r), waviness (Sa,w), and

water contact angle were measured. Three measurements were taken and averaged for all the response variables. Table 1: Main specifications of the employed laser system.

Wavelength	λ	1,064 nm
Max average power	P_{avg}	50 W
Pulse repetition rate	PRR	20-80 kHz
Max pulse energy	E_{max}	1 mJ
Pulse duration	τ_{on}	250 ns
Beam quality	M^2	1.7
Collimated beam diameter	d_c	5.9 mm
Focusing lens	f	100 mm
Focused beam diameter	d_0	39 µm

Table 2 summarizes each parameter defined in the experimental plan, classifying fixed, varied parameters and measured variables. Statistical analysis was carried out on the measured data to identify the significant process parameters, and a regression model was sought to provide a good fit between the process parameters and the surface topography parameters. The models were used to depict the trend in the change of Sa,r and Sa,w as a function of significant process parameters. The models were also used to identify the highest and lowest Sa,r and Sa,w. These conditions were then further analysed to identify the effect of the process on the bacterial cleanibility along with the untreated surface.

2.4.2 Surface cleanability

Surface cleanability was evaluated through bacterial adhesion tests with regard to the specific application. *E. coli*, a bacterium typically 2 µm long and 0.5 µm wide, was used to carry out this experiments. In this context, tests were designed to evaluate the number of adherent bacteria and other possible contaminants after washing. In particular, the experimental activity about surface cleanibility was carried out following three main steps:

1. Bacterial suspension was settled directly onto samples;
2. Samples were washed with a selected washing solution;
3. Samples were analysed to evaluate the number of particles adhering on their surface.

Bacterial concentration, the composition of the washing solution and the washing time were held constant. For all adhesion tests, *E. coli* JM109 strain was streaked out with a loop from the 15% glycerol frozen stock and grown in 5 mL LB (Luria-Bertani) Broth at 37°C under shaking at 140 rpm till mid-exponential phase. The stainless steel surfaces were sterilized and placed in a sterile 24-well plate with 600 µL bacterial suspension properly diluted (10-20 cells/mm^2) and then incubated at 37°C for 2 hrs. Stainless steel surfaces were next removed and thoroughly rinsed (25°C, 175 rpm) with 1 mL of "washing solution" (0.1% v/v Triton X-100 in 0.5 M NaCl) to remove the excess of bacteria only loosely bound to surfaces. Each stainless steel surface was taken out and underwent SEM acquisitions to allow counting the number of adherent

bacteria. Adherent bacteria were also counted after nuclear staining with DAPI by means of a fluorescence microscope (BX51WI from Olympus, Tokyo, Japan). Three acquisitions and counts were carried out for each surface type.

The test consisted in two different phases:

i) Effect of LμP conditions on surface cleanability. Conditions with the lowest (S1) and the highest (S2) surface roughness were investigated and compared to untreated surfaces. Tests were carried out with fixed washing time of 1 hr. Circular stainless steel surfaces with Ø=15 mm underwent laser micropolished. Table 1: Main specifications of the employed laser system.

Wavelength	λ	1,064 nm
Max average power	P_{avg}	50 W
Pulse repetition rate	PRR	20-80 kHz
Max pulse energy	E_{max}	1 mJ
Pulse duration	τ_{on}	250 ns
Beam quality	M^2	1.7
Collimated beam diameter	d_c	5.9 mm
Focusing lens	f	100 mm
Focused beam diameter	d_0	39 μm

Table 2: Experimental plan for L*μ*P treatments.

Fixed parameters		Levels
Pulse repetition rate	PRR [kHz]	65
Pitch	p [μm]	10
Defocusing	Δz [mm]	2
Gas type		N_2
Gas pressure	[bar]	0.3

Varied parameters		Levels
Laser energy	E [mJ]	0.19, 0.28, 0.38, 0.47
Scanning speed	v [m/min]	12, 24, 48, 96, 192
Number of passes	N	1, 2, 4

Measured variables	
Surface roughness	Sa,r [nm]
Surface waviness	Sa,w [nm]
Surface wettability	Contact angle [°]

ii) Table 3 summarizes each parameter defined in the experimental plan adopted in phase i), classifying fixed, varied parameters and measured variables.

iii) Effect of washing time on the cleanability of LμP surface. The lowest surface roughness condition (S1), which was identified as the best LμP condition in the previous phase was compared to the untreated surface (B). Circular stainless steel surfaces with Ø=15 mm were half laser micropolished and half untreated (control surfaces). Washing time was varied from 15 to 120 min. All conditions were replicated three times. Table 4 summarizes each parameter defined in phase ii), classifying fixed

and varied parameters.

3. Results and discussions

3.1. Laser micropolished surface morphology

The effects of process parameters on surface morphology are shown in Figure 1. It is worthy to note that scan speed and pulse energy provide substantial changes in the surface morphology, whereas the effect of number of passes is less marked. Besides, the higher the scanning speed results in an incomplete polishing process as some grain boundaries remain on surfaces. This effect, obviously, decreases with increasing the energy. In a similar fashion, the lowest scanning speed values induce some defects on surface, such as holes, asperities and microwaviness expected to be due to the molten material instabilities. In particular, the effect of speed on defects is stronger for higher energy value.

The effect of number of passes can be visualized in Figure 1. The morphological changes due to increased number of passes are evident on the highest and lowest energetic conditions. In particular, increased number of passes appears to remove the incomplete surface polishing obtained at high scan speeds with low pulse energy. For low scan speed and high pulse energy combinations surface topography appears modified.

Despite a general improvement in the surface roughness, the LμP process generated also different types of defects under the different parameter combinations. Figure 1: Effect of process parameters on surface morphology. A) N=1 means single pass; B) N=4, four passes.

Figure 2 gathers the different classes of defects observed. Incomplete polishing occurs at low energy input, characterised by low pulse energy and number of passes with high scan speed (see Figure 1: Effect of process parameters on surface morphology. A) N=1 means single pass; B) N=4, four passes.

Figure 2.B). Microholes with diameters in the order of a few μm occur when high energy input is present with process parameters set at the opposite extreme compared to incomplete polishing (see Figure 1: Effect of process parameters on surface morphology. A) N=1 means single pass; B) N=4, four passes.

Figure 2.C). Surface roughness increases due to the generation of microwaviness (see Figure 1: Effect of process parameters on surface morphology. A) N=1 means single pass; B) N=4, four passes.

Figure 2.D) and molten asperities (see Figure 1: Effect of process parameters on surface morphology. A) N=1 means single pass; B) N=4, four passes.

Figure 2.E), which appear at high pulse energy conditions. The use of moderate process parameters allows for obtaining defect-free polished surfaces (see Figure 1: Effect of process parameters on surface morphology. A) N=1 means single pass; B) N=4, four passes.

Figure 2.F). The phenomenon of defect growth was previously highlighted by Nüsser et al., who showed that even win certain conditions the process could add another roughness component to the initial surface profile [15]. On the other hand, the interface between untreated and polished surface is shown in Figure 1:

Effect of process parameters on surface morphology. A) N=1 means single pass; B) N=4, four passes.

Figure 2.G. Under stable polishing conditions, the molten material fills in the surface cracks realized by the rolling process. The incomplete polishing conditions are expected to be due to intermittent melting action due to decreased overlapping between adjacent molten zones. It should be noted that the extent of the molten zone can be much smaller than the beam size over the material surface. This is due to the reduced coupling between the laser beam and the processed material, when low energy conditions are present. Once this coupling is established, a constant melt track can be achieved, which gives rise to a homogenous polished zone. Increased pulse energy and lowered scan speeds can cause excessive melting and liquid instabilities forming the various defects.

3.2. Surface roughness and waviness

The surface roughness could be lowered to Sa,r=36 nm and Sa,w=35 nm at minimum, corresponding to a decrease of approximately 58% and 38% in average surface roughness and waviness respectively. On the other hand, the same process increased surface waviness in non-optimal conditions with Sa,w values as high as approximately 200 nm.

The main effects plots in Figure 1: Effect of process parameters on surface morphology. A) N=1 means single pass; B) N=4, four passes.

Figure 2: Defects classification: A) Bulk material; B) Unremoved grain boundaries (0.19 mJ, 192 m/min, N=1); C) Holes (0.28 mJ, 24 m/min, N4); D) Microwaviness (0.47 mJ, 24 m/min, N=1); E) Molten asperities (0.38 mJ, 96 m/min, N=4); F) Polished (0.19 mJ, 48 m/min, N=1); G) Interface between non-treated and polished surface.

Figure 3 reports the mean Sa,r and Sa,w measurements for every factor level. The graphs depict the effect of each single factor on the response value, without considering the effect of possible interactions among them. The plots confirm that pulse energy and scan speed are the main factors over the surface roughness and waviness. On the measured response values, Sa,r and Sa,w, follow a growing trend as a function of the pulse energy (see Figure 1: Effect of process parameters on surface morphology. A) N=1 means single pass; B) N=4, four passes.

Figure 2: Defects classification: A) Bulk material; B) Unremoved grain boundaries (0.19 mJ, 192 m/min, N=1); C) Holes (0.28 mJ, 24 m/min, N4); D) Microwaviness (0.47 mJ, 24 m/min, N=1); E) Molten asperities (0.38 mJ, 96 m/min, N=4); F) Polished (0.19 mJ, 48 m/min, N=1); G) Interface between non-treated and polished surface.

Figure 3.A and Figure 1: Effect of process parameters on surface morphology. A) N=1 means single pass; B) N=4, four passes.

Figure 2: Defects classification: A) Bulk material; B) Unremoved grain boundaries (0.19 mJ, 192 m/min, N=1); C) Holes (0.28 mJ, 24 m/min, N4); D) Microwaviness (0.47 mJ, 24 m/min, N=1); E) Molten asperities (0.38 mJ, 96 m/min, N=4); F) Polished (0.19 mJ, 48 m/min, N=1); G) Interface between non-treated and polished surface.

Figure 3.B). It has been previously shown that final polished roughness decreases when laser power increased until a certain value. With further increase of laser power, the trend was inverted, i.e. increasing of

laser power resulted in increasing of roughness [11],[21]. The results shown in our study are consistent with the previous observations.

The main effect of scan speed on the response variables follows a parabolic trend (Figure 1: Effect of process parameters on surface morphology. A) N=1 means single pass; B) N=4, four passes.

Figure 2: Defects classification: A) Bulk material; B) Unremoved grain boundaries (0.19 mJ, 192 m/min, N=1); C) Holes (0.28 mJ, 24 m/min, N4); D) Microwaviness (0.47 mJ, 24 m/min, N=1); E) Molten asperities (0.38 mJ, 96 m/min, N=4); F) Polished (0.19 mJ, 48 m/min, N=1); G) Interface between non-treated and polished surface.

Figure 3.C, Figure 1: Effect of process parameters on surface morphology. A) N=1 means single pass; B) N=4, four passes.

Figure 2: Defects classification: A) Bulk material; B) Unremoved grain boundaries (0.19 mJ, 192 m/min, N=1); C) Holes (0.28 mJ, 24 m/min, N4); D) Microwaviness (0.47 mJ, 24 m/min, N=1); E) Molten asperities (0.38 mJ, 96 m/min, N=4); F) Polished (0.19 mJ, 48 m/min, N=1); G) Interface between non-treated and polished surface.

Figure 3.D). While for Sa,r the smallest values appear around intermediate scan speeds, higher speeds tend to further decrease Sa,w.

Number of passes shows very little change over the response variables (Figure 1: Effect of process parameters on surface morphology. A) N=1 means single pass; B) N=4, four passes.

Figure 2: Defects classification: A) Bulk material; B) Unremoved grain boundaries (0.19 mJ, 192 m/min, N=1); C) Holes (0.28 mJ, 24 m/min, N4); D) Microwaviness (0.47 mJ, 24 m/min, N=1); E) Molten asperities (0.38 mJ, 96 m/min, N=4); F) Polished (0.19 mJ, 48 m/min, N=1); G) Interface between non-treated and polished surface.

Figure 3.E, Figure 1: Effect of process parameters on surface morphology. A) N=1 means single pass; B) N=4, four passes.

Figure 2: Defects classification: A) Bulk material; B) Unremoved grain boundaries (0.19 mJ, 192 m/min, N=1); C) Holes (0.28 mJ, 24 m/min, N4); D) Microwaviness (0.47 mJ, 24 m/min, N=1); E) Molten asperities (0.38 mJ, 96 m/min, N=4); F) Polished (0.19 mJ, 48 m/min, N=1); G) Interface between non-treated and polished surface.

Figure 3.F). This can be attributed to the fact that the process is stable between different passes. After the first pass, the surface is asperities are filled reducing surface roughness and waviness overall. Another important factor is that the polished surface after the first pass is expected to induce higher reflectivity to the incident laser light, which can reduce the absorbed amount of energy in the successive passes. Therefore, surface remelting is expected to occur at a lower extent. Indeed, other surface measurements such as the ones employing surface autocorrelation may resolve the effect of this parameter over the change of homogeneity of the surface texture.

Statistical analysis was carried out to better quantify the effects of the process parameters and regression models were fitted for Sa,r and Sa,w. The significant factors are energy E, scanning speed v, their second order interaction E*v, the second order term E^2 and v^2. For Sa,w also the constant term results significant for regression models. Number of passes was not significant coherently with the previous observations.

The plots of fitted regression models are represented in Figure 4 and the respective equations are given in **Error! Reference source not found.**. The high R^2_{adj} values reveal the reliability of regression models that fit experimental data well. The plots put into evidence that in all the conditions Sa,r is effectively reduced, whereas the Sa,w can be increased compared to the non-treated surface. On the other hand, the conditions for minimum and maximum values of Sa,r and Sa,w can be deduced from Figure 4 as the saddle points. The

minimum value both for Sa,r and for Sa,w could be placed for E of 0.19 mJ and v from 48 to 138 m/min. The maximum value both for Sa,r and for Sa,w could be placed for E of 0.47 mJ and v from 12 to 30 m/min.

Figure 1: Effect of process parameters on surface morphology. A) N=1 means single pass; B) N=4, four passes.

Figure 2: Defects classification: A) Bulk material; B) Unremoved grain boundaries (0.19 mJ, 192 m/min, N=1); C) Holes (0.28 mJ, 24 m/min, N4); D) Microwaviness (0.47 mJ, 24 m/min, N=1); E) Molten asperities (0.38 mJ, 96 m/min, N=4); F) Polished (0.19 mJ, 48 m/min, N=1); G) Interface between non-treated and polished surface.

Figure 3: Main effects of laser parameters on Sa,r and Sa,w: A), B) and E) represents Sa,r as a function of E, v and N, while B), D) and F) represents Sa,w as a function of E, v, N.

Figure 4: Graphs of implemented regression models: A) Sa,r; B) Sa,w.

Figure 5 compares the Sa,r and Sa,w measurement couples of each condition. The dotted red lines correspond to surface characteristics of the untreated surface, dividing the graph into four different areas. The change in surface roughness and waviness appear to be linked. The lower-left quadrant of the graph represents conditions in which both surface roughness and waviness are lowered. The main evidence is that LμP seems to be more efficient for roughness reduction rather than waviness. The larger portion of the experimental conditions stand in the region in which surface roughness is lowered, whereas surface waviness is increased. As a matter of fact, almost all of the conditions are characterized by a lower Sa,r value than that of untreated surface, up to a reduction of 58% (from 85.33 nm to 34.45 nm). This is due to the closure of the surface cracks and rolling texture. However, waviness variations depend also on how the molten material during the LμP process is redistributed on the surface. Indeed, the motion of the molten pool is effective on the final result. Perry et al. have proposed a model to predict the final roughness/waviness of metal surfaces that have undergone laser polishing. They showed that LμP process can smoothen the surface profile waviness components until a critical wavelength, beyond which the waviness increases as a function of laser process parameters [14], [22], [23].

3.3. Surface wettability

Figure 1: Effect of process parameters on surface morphology. A) N=1 means single pass; B) N=4, four passes.

Figure 2: Defects classification: A) Bulk material; B) Unremoved grain boundaries (0.19 mJ, 192 m/min, N=1); C) Holes (0.28 mJ, 24 m/min, N4); D) Microwaviness (0.47 mJ, 24 m/min, N=1); E) Molten asperities (0.38 mJ, 96 m/min, N=4); F) Polished (0.19 mJ, 48 m/min, N=1); G) Interface between non-treated and polished surface.

Figure 3: Main effects of laser parameters on Sa,r and Sa,w: A), B) and E) represents Sa,r as a function of E, v and N, while B), D) and F) represents Sa,w as a function of E, v, N.

Figure 4: Graphs of implemented regression models: A) Sa,r; B) Sa,w.

Figure 5: Sa,r and Sa,w measured values for all treatments.

Figure 6 shows the measured contact angles as a function of surface roughness Sa,r and waviness Sa,w. It is apparent that LμP treatments induced a more hydrophobic behaviour as compared to the parent material. Contact angle increased up to approximately 110°. No clear relationship between the surface roughness and waviness can be found. This can be attributed to the fact that the surface topography after LμP is expected to be significantly different from the initial surface. However, the surface topography does not vary significantly between conditions to induce any change in wettability. Cassie-Baxter wettability model describes the relationship between surface roughness and contact angle:

$$\cos\theta_r = r\cos\theta_f \quad (1)$$

where θ_f is the contact angle of a flat surface, θ_r is the contact angle of rough surface and r is the roughness factor that is the ratio between effective surface area and an ideally flat surface area with r>1. According to the model, reducing the surface roughness of a hydrophilic surface would increase the contact angle towards the contact angle of the flat surface, which will theoretically be below 90° at maximum. The results indicate that the contact angle varies around this limit of 90°, depicting the saturation limit by the reduction in surface area.

3.4. Surfaces selection

The thorough characterization of polished surfaces allowed to identify the best candidates for chemical composition analysis and for cleanability tests. According to general antibacterial requirements, the surface with the lowest roughness values (S1) was chosen. As antithetical counterpart, the roughest condition (S2) was tested as well. This way the influence of topography also within the laser micropolished surface can be assessed (

). As control, untreated surface material was used (B). In particular, the treated conditions analysed were derived through the minimization and maximization of the implemented regression models (Figure 4 and **Error! Reference source not found.**):

- S1: E = 0.19 mJ, v = 48 m/min, N_2
- S2: E = 0.47 mJ, v = 12 m/min, N_2

reports the topography measurements and SEM micrographs of the three selected surfaces. Figure 8 summarizes their wetting behaviour and shows the increase in surface hydrophobicity after LμP.

3.5. Surface chemical composition

Error! Reference source not found. shows the EDS analysis of chemical composition, while Figure 10 reports XRD spectra for the three analysed surfaces. As seen in **Error! Reference source not found.**, no significant difference in the chemical composition was observed among the three selected samples. No significant increase of surface nitrides was observed, confirming that the N_2 process gas held a shielding effect only.

About XRD tests, in all tested conditions the spectra show chromium-iron-nickel austenitic stainless steel with the five peaks defined marked in the graph. Laser treated surfaces S1 and S2 show the same five peaks in the same positions of untreated surface B. This means that there is not any variation in chemical composition after LμP treatments. The broadening and the rise of the observed peaks indicates a general reduction in the grain size [24]. The grain refinement is expected to occur due to the fast cooling cycle induced in the process. The change in the peak intensity increases moving towards higher energy conditions, *i.e.* from S1 to S2. This is attributed to the fact that with higher pulse energy and lower scan speed. LμP takes effect in a larger depth refining the grains. Altogether, these analyses highlight that the LμP process provides modification on surface topography without altering the surface chemistry.

3.6. Surface cleanability

Figure 1: Effect of process parameters on surface morphology. A) N=1 means single pass; B) N=4, four passes.

Figure 2: Defects classification: A) Bulk material; B) Unremoved grain boundaries (0.19 mJ, 192 m/min, N=1); C) Holes (0.28 mJ, 24 m/min, N4); D) Microwaviness (0.47 mJ, 24 m/min, N=1); E) Molten asperities (0.38 mJ, 96 m/min, N=4); F) Polished (0.19 mJ, 48 m/min, N=1); G) Interface between non-treated and polished surface.

Figure 3: Main effects of laser parameters on Sa,r and Sa,w: A), B) and E) represents Sa,r as a function of E, v and N, while B), D) and F) represents Sa,w as a function of E, v, N.

Figure 4: Graphs of implemented regression models: A) Sa,r; B) Sa,w.

Figure 5: Sa,r and Sa,w measured values for all treatments.

Figure 6: Contact angle measurements as a function of Sa,r (A) and Sa,w (B).

Figure 7: SEM images (A) for B, B) for S1 and C) for S2) and roughness/waviness parameters (D) of the three selected surfaces for bacteria adhesion tests. Error bars represent standard deviation of the measurements.

Figure 8: Wettability of the three selected surfaces for bacteria adhesion tests. Error bars represent standard deviation of the measurements.

Figure 9: EDS analysis of chemical composition for the three selected surfaces B, S1 and S2.

Figure 10: XRD spectra for the three selected surfaces B, S1 and S2. The indexed peaks with asterisk indicate chromium-iron-nickel austenitic stainless steel.

Figure 11 depicts SEM images of the surfaces after the first cleanability test. From the observation of these SEM micrographs, it is evident the presence of precipitates on surfaces, which are not bacteria. Since the washing solution contains 0.5 M NaCl, such deposits are likely to be salt crystals. Nevertheless, the main evidence from Figure 1: Effect of process parameters on surface morphology. A) N=1 means single pass; B) N=4, four passes.

Figure 2: Defects classification: A) Bulk material; B) Unremoved grain boundaries (0.19 mJ, 192 m/min, N=1); C) Holes (0.28 mJ, 24 m/min, N4); D) Microwaviness (0.47 mJ, 24 m/min, N=1); E) Molten asperities (0.38 mJ, 96 m/min, N=4); F) Polished (0.19 mJ, 48 m/min, N=1); G) Interface between non-treated and polished surface.

Figure 3: Main effects of laser parameters on Sa,r and Sa,w: A), B) and E) represents Sa,r as a function of E, v and N, while B), D) and F) represents Sa,w as a function of E, v, N.

Figure 4: Graphs of implemented regression models: A) Sa,r; B) Sa,w.

Figure 5: Sa,r and Sa,w measured values for all treatments.

Figure 6: Contact angle measurements as a function of Sa,r (A) and Sa,w (B).

Figure 7: SEM images (A) for B, B) for S1 and C) for S2) and roughness/waviness parameters (D) of the three selected surfaces for bacteria adhesion tests. Error bars represent standard deviation of the measurements.

Figure 8: Wettability of the three selected surfaces for bacteria adhesion tests. Error bars represent standard deviation of the measurements.

Figure 9: EDS analysis of chemical composition for the three selected surfaces B, S1 and S2.

Figure 10: XRD spectra for the three selected surfaces B, S1 and S2. The indexed peaks with asterisk indicate chromium-iron-nickel austenitic stainless steel.

Figure 11 is that:

i) Particles are retained in grain boundaries that characterized the untreated surface B;

ii) Particles spread uniformly on the whole area of treated surface S2;

iii) Treated S1 surface is the cleanest one.

These results underline how roughness and waviness reduction, as well as grain boundaries removal, induce the overall cleanability of laser micropolished surfaces. In fact, as for salt deposits, also bacteria may be retained in possible surface irregularities. In this way, single bacteria could cluster together and form colonies that are more difficult to be removed from grain boundaries that protect them from unfavourable environmental factors and shear stress of washing. Therefore, the surface smoothing and the grain boundaries removal induced by LμP process are supposed to have a direct bearing in cleanability.

The results herein reported are in agreement with other recent reports that demonstrated how bacteria preferentially adhere to rougher surfaces. Whitehead and Verran underlined how smooth stainless steel is more hygienic than the rougher one [4]. Others investigated the effect of surface morphology, obtaining different bacterial coverages that were 59% for a satin-finished titanium surface (Ra=0.83 μm) and 52% for a grit-blasted surface (Ra=11 μm), while around 10% for polished surfaces (Ra=0.006 μm) and plasma-sprayed titanium (Ra=33 μm) [2]. Yoda et al. prepared specimens of pure metals and alloys that divided into two groups depending on different surface finishes: the fine group (Ra=1.8-8.5 nm, <10 nm) and the coarse group (Ra=7.2-30.0 nm) [3]. Interestingly, a greater amount of bacteria adhered to coarse specimens as compared to the fine group. Building et al. studied the adhesion to polymethylmethacrylate (PMMA) surfaces with Ra in the range of 0.04-7.89 μm and showed that bacterial adhesion increased between 0.3 and 1.86 μm, whereas smoother or rougher surfaces displayed low bacterial coverage [7]. Moreover, Mei et al.

compared bacterial attachment on two orthodontic composite resins after polishing (smooth with Ra=20 nm) and after grinding (rough with Ra=350 nm) and noticed that streptococcal adhesion increased with increasing roughness of the composite surfaces [5]. On the other hand, surface hydrophobicity may also play an important role in the bacterial adhesion process as well as on cleaning action in the way that hydrophilic surfaces do attract bacteria [9]. Conversely, highly hydrophobic surfaces show self-cleaning capability, which allows ease of particle removal.

The images in Figure 1: Effect of process parameters on surface morphology. A) N=1 means single pass; B) N=4, four passes.

Figure 2: Defects classification: A) Bulk material; B) Unremoved grain boundaries (0.19 mJ, 192 m/min, N=1); C) Holes (0.28 mJ, 24 m/min, N4); D) Microwaviness (0.47 mJ, 24 m/min, N=1); E) Molten asperities (0.38 mJ, 96 m/min, N=4); F) Polished (0.19 mJ, 48 m/min, N=1); G) Interface between non-treated and polished surface.

Figure 3: Main effects of laser parameters on Sa,r and Sa,w: A), B) and E) represents Sa,r as a function of E, v and N, while B), D) and F) represents Sa,w as a function of E, v, N.

Figure 4: Graphs of implemented regression models: A) Sa,r; B) Sa,w.

Figure 5: Sa,r and Sa,w measured values for all treatments.

Figure 6: Contact angle measurements as a function of Sa,r (A) and Sa,w (B).

Figure 7: SEM images (A) for B, B) for S1 and C) for S2) and roughness/waviness parameters (D) of the three selected surfaces for bacteria adhesion tests. Error bars represent standard deviation of the measurements.

Figure 8: Wettability of the three selected surfaces for bacteria adhesion tests. Error bars represent standard deviation of the measurements.

Figure 9: EDS analysis of chemical composition for the three selected surfaces B, S1 and S2.

Figure 10: XRD spectra for the three selected surfaces B, S1 and S2. The indexed peaks with asterisk indicate chromium-iron-nickel austenitic stainless steel.

Figure 11 show that S1 treatment provides the cleanest surface. Therefore, in the second phase of our study, S1 treatment was compared to untreated surface B at varying washing times. After washing, the number of remaining bacteria was counted on each half specimen and expressed in terms of bacteria sticking to the surface. Figure 1: Effect of process parameters on surface morphology. A) N=1 means single pass; B) N=4, four passes.

Figure 2: Defects classification: A) Bulk material; B) Unremoved grain boundaries (0.19 mJ, 192 m/min, N=1); C) Holes (0.28 mJ, 24 m/min, N4); D) Microwaviness (0.47 mJ, 24 m/min, N=1); E) Molten asperities (0.38 mJ, 96 m/min, N=4); F) Polished (0.19 mJ, 48 m/min, N=1); G) Interface between non-treated and polished surface.

Figure 3: Main effects of laser parameters on Sa,r and Sa,w: A), B) and E) represents Sa,r as a function of E, v and N, while B), D) and F) represents Sa,w as a function of E, v, N.

Figure 4: Graphs of implemented regression models: A) Sa,r; B) Sa,w.

Figure 5: Sa,r and Sa,w measured values for all treatments.

Figure 6: Contact angle measurements as a function of Sa,r (A) and Sa,w (B).

Figure 7: SEM images (A) for B, B) for S1 and C) for S2) and roughness/waviness parameters (D) of the three selected surfaces for bacteria adhesion tests. Error bars represent standard deviation of the measurements.

Figure 8: Wettability of the three selected surfaces for bacteria adhesion tests. Error bars represent standard deviation of the measurements.

Figure 9: EDS analysis of chemical composition for the three selected surfaces B, S1 and S2.

Figure 10: XRD spectra for the three selected surfaces B, S1 and S2. The indexed peaks with asterisk indicate chromium-iron-nickel austenitic stainless steel.

Figure 11: SEM images after first bacteria adhesion tests and relative focus variation microscope acquisitions (110.61×145.81 μm^2): A) for B, B) for S1 and C) for S2.

Figure 12 reports the ratio of bacteria remaining on treated and untreated specimens as a function of washing time. Notably, bacteria adhesion is more pronounced on untreated halves and thus the percentage of cells on the treated surface was invariably lower at every time point. On average, the number of bacteria sticking to the untreated surface is 5 times higher than that of the LμP specimen. Analysis of variance (ANOVA) confirms that while the treatment was largely effective, the washing duration had no significant effect on the final outcome (p-value>0.05), whereas the surface type is effective in cleanability (p-value<0.05). Figure 13 depicts fluorescent microscopy images of the bacteria remaining on the surfaces after washing. A higher number of bacteria is visible on untreated surfaces, in some cases in the form of larger clusters, as compared to LμP surfaces.

4. Conclusions

This work reports the study of LμP process to serve for surface functionalization and specially to improve cleanability properties, obtaining:

- Surface finishing improvement and more hydrophobic behaviour.
- Enhanced cleanability properties on polished surfaces.

The LμP process was studied using an industrial pulsed fibre laser operating in ns-pulse regime on AISI 304 stainless steel, a material commonly used in food industry and kitchen equipment. The process was carried out under controlled atmosphere using N_2 as process gas. The improvement of the surfaces finishing focused mainly on surface smoothing and grain boundaries removal. The importance of this result is more evident considering the already good initial roughness of material for the previous cold rolled treatment. Indeed, starting from a Sa,r=85 nm for untreated surfaces, a roughness reduction up to 60% was achieved after polishing (Sa,r=35 nm). Surface defects generated during the different LμP processing conditions were identified and analysed as well. The obtained results disclose that the LμP process is characterized by a small feasibility window in which both surface roughness and waviness can be reduced. This corresponded to pulse energy levels around 0.19 mJ and scan speeds between 24-60 m/min for the employed material. Surface smoothing was accompanied by an increase of water contact angle from 49°±4° of untreated to 96°±8° LμP treated surfaces. The surface chemistry did not show any significant difference between laser treated surfaces and the untreated one.

On the other hand, surface cleanability was assessed through bacteria adhesion tests, carried out on two selected treated surfaces and on the untreated material. Thus, untreated surfaces with wider scratches and grain boundaries did exhibit a higher fraction of bacteria and other possible particles retained, while the smoothest LμP surfaces exhibited a random particle distribution. This difference was probably due to the fact that non-treated surfaces had more attachment sites, a larger surface contact area and topographical

features that reduced the cleaning shear force. The best between the different LμP surfaces was found to be the one with reduced surface roughness (Sa,r=35 nm; Sa,w=41 nm) and it proved to retain five times less bacteria with respect to untreated surfaces, regardless of the washing time. This means that the enhanced cleanability of the LμP surfaces is referable just to roughness reduction and increased hydrophobicity, rather than to surface chemistry changes.

The present work confirms the feasibility of using the LμP process for the production and optimization of high cleanable and antibacterial surfaces. However, its industrialization requires processing of large surfaces in relatively short times and these aspects seem to be major drawbacks. In this regard, process upscaling can be achieved by using larger beams and beam shaping techniques for parallel processing. Another possibility that is readily available is the use of multiple processing heads with a single laser source. Given the fact that the process requires little laser energy, beam sharing of a high energy laser source seems the most promising alternative for higher productivity.

References

[1] D. Campoccia, L. Montanaro, and C. R. Arciola,;1; "A review of the biomaterials technologies for infection-resistant surfaces.," *Biomaterials*, vol. 34, no. 34, pp. 8533–54, Nov. 2013.

[2] Y. Wu, J.P. Zitelli, K.S. TenHuisen, X. Yu, and M. R. Libera,;1; "Differential response of Staphylococci and osteoblasts to varying titanium surface roughness.," *Biomaterials*, vol. 32, no. 4, pp. 951–60, Feb. 2011.

[3] I. Yoda, H. Koseki, M. Tomita, T. Shida, H. Horiuchi, H. Sakoda, and M. Osaki,;1; "Effect of surface roughness of biomaterials on Staphylococcus epidermidis adhesion.," *BMC Microbiol*., vol. 14, p. 234, Jan. 2014.

[4] K. a. Whitehead and J. Verran,;1; "The Effect of Surface Topography on the Retention of Microorganisms," *Food Bioprod*. *Process*., vol. 84, no. 4, pp. 253–259, Dec. 2006.

[5] L. Mei, H.J. Busscher, H.C. van der Mei, and Y. Ren,;1; "Influence of surface roughness on streptococcal adhesion forces to composite resins.," *Dent*. *Mater*., vol. 27, no. 8, pp. 770–8, Aug. 2011.

[6] L. R. Hilbert, D. Bagge-Ravn, J. Kold, and L. Gram,;1; "Influence of surface roughness of stainless steel on microbial adhesion and corrosion resistance," *Int*. *Biodeterior*. *Biodegradation*, vol. 52, no. 3, pp. 175–185, Oct. 2003.

[7] J. D. Building and O. Road,;1; "The influence of substratum topography on bacterial adhesion to polymethyl methacrylate," vol. 9, pp. 17–22, 1998.

[8] C. Desrousseaux, V. Sautou, S. Descamps, and O. Traoré,;1; "Modification of the surfaces of medical devices to prevent microbial adhesion and biofilm formation.," *J*. *Hosp*. *Infect*., vol. 85, no. 2, pp. 87–93, Oct. 2013.

[9] X. Zhang, L. Wang, and E. Levänen,;1; "Superhydrophobic surfaces for the reduction of bacterial adhesion," *RSC Adv*., vol. 3, no. 30, p. 12003, 2013.

[10] E. V. Bordatchev, A.M. K. Hafiz, and O. R. Tutunea-Fatan,;1; "Performance of laser polishing in finishing of metallic surfaces," *Int*. *J*. *Adv*. *Manuf*. *Technol*., vol. 73, no. 1–4, pp. 35–52, Apr. 2014.

[11] T. a. Mai and G. C. Lim,;1; "Micromelting and its effects on surface topography and properties in laser polishing of stainless steel," *J*. *Laser Appl*., vol. 16, no. 4, p. 221, 2004.

[12] A. Temmler, E. Willenborg, and K. Wissenbach,;1; "Design Surfaces by Laser Remelting," *Phys*. *Procedia*, vol. 12, pp. 419–430, 2011.

[13] V. M. Yermachenko, Y.A. Vdovin, V.D. Mironov, N. V Naumov, V.N. Petrovskiy, N.M. Prokopova, V.I. Polsky, P.S. Dzhumaev, and V. L. Yakushin,;1; "Technology of Polishing of Titanium Surface Using the Fiber Laser Radiation," vol. 20, no. 6, pp. 1537–1544, 2010.

[14] T. L. Perry, D. Werschmoeller, X. Li, F.E. Pfefferkorn, and N. a. Duffie,;1; "Pulsed laser polishing of micro-milled Ti6Al4V samples," *J. Manuf. Process.*, vol. 11, no. 2, pp. 74–81, Jul. 2009.

[15] C. Nüsser, J. Kumstel, T. Kiedrowski, A. Diatlov, and E. Willenborg,;1; "Process- and Material-Induced Surface Structures During Laser Polishing," *Adv. Eng. Mater.*, vol. 17, no. 3, pp. 268–277, 2015.

[16] ;1; *Food Processing: Understanding and Controlling E. Coli Contamination*. The Hartford, Loss Control Deparment, 1998.

[17] ;1; "ASME B46.1-2002: Surface Texture (Surface roughness, Waviness, and Lay)," 2004.

[18] C. De Giorgi, V. Furlan, A.G. Demir, E. Tallarita, G. Candiani, and B. Previtali,;1; "Laser micro-polishing of stainless steel for antibacterial surface applications," *Sci. Second CIRP Conf. Biomanufacturing*, 2015.

[19] L.-H. Lin, S.-C. Chen, C.-Z. Wu, J.-M. Hung, and K.-L. Ou,;1; "Microstructure and antibacterial properties of microwave plasma nitrided layers on biomedical stainless steels," *Appl. Surf. Sci.*, vol. 257, no. 17, pp. 7375–7380, Jun. 2011.

[20] H. Wang, J. Ji, W. Zhang, W. Wang, Y. Zhang, Z. Wu, Y. Zhang, and P. K. Chu,;1; "Rat calvaria osteoblast behavior and antibacterial properties of O(2) and N(2) plasma-implanted biodegradable poly(butylene succinate).," *Acta Biomater.*, vol. 6, no. 1, pp. 154–9, Jan. 2010.

[21] K. Alrbaey, D. Wimpenny, R. Tosi, W. Manning, and a. Moroz,;1; "On Optimization of Surface Roughness of Selective Laser Melted Stainless Steel Parts: A Statistical Study," *J. Mater. Eng. Perform.*, vol. 23, no. 6, pp. 2139–2148, Apr. 2014.

[22] T. L. Perry, N.A. Duffie, and F. E. Pfefferkorn,;1; "Examination of Selective Pulsed Laser Micropolishing on Microfabricated Nickel Samples Using Spatial Frequency Analysis," vol. 131, no. April 2009, pp. 1–9, 2015.

[23] T. L. Perry, F.E. Pfefferkorn, and N. A. Duffie,;1; "The Effect of Laser Pulse Duration and Feed Rate on Pulsed Laser Polishing of Microfabricated," vol. 131, no. June 2009, pp. 1–7, 2014.

[24] C.E. Kril and R. Birringer,;1; " Estimating grain-size distributions in nanocrystalline materials from X-ray diffraction profile analysis", Philosophical Magazine A, vol. 77, no. 3, 621-640, 1997.

Figures caption

Figure 1: Effect of process parameters on surface morphology. A) N=1 means single pass; B) N=4, four passes.

Figure 2: Defects classification: A) Bulk material; B) Unremoved grain boundaries (0.19 mJ, 192 m/min, N=1); C) Holes (0.28 mJ, 24 m/min, N4); D) Microwaviness (0.47 mJ, 24 m/min, N=1); E) Molten asperities (0.38 mJ, 96 m/min, N=4); F) Polished (0.19 mJ, 48 m/min, N=1); G) Interface between non-treated and polished surface.

Figure 3: Main effects of laser parameters on Sa,r and Sa,w: A), B) and E) represents Sa,r as a function of E, v and N, while B), D) and F) represents Sa,w as a function of E, v, N.

Figure 4: Graphs of implemented regression models: A) Sa,r; B) Sa,w.

Figure 5: Sa,r and Sa,w measured values for all treatments.

Figure 6: Contact angle measurements as a function of Sa,r (A) and Sa,w (B).

Figure 7: SEM images (A) for B, B) for S1 and C) for S2) and roughness/waviness parameters (D) of the three selected surfaces for bacteria adhesion tests. Error bars represent standard deviation of the measurements.

Figure 8: Wettability of the three selected surfaces for bacteria adhesion tests. Error bars represent standard deviation of the measurements.

Figure 9: EDS analysis of chemical composition for the three selected surfaces B, S1 and S2.

Figure 10: XRD spectra for the three selected surfaces B, S1 and S2. The indexed peaks with asterisk indicate chromium-iron-nickel austenitic stainless steel.

Figure 11: SEM images after first bacteria adhesion tests and relative focus variation microscope acquisitions (110.61×145.81 μm^2): A) for B, B) for S1 and C) for S2.

Figure 12: Percentage of adherent bacteria on B and S1 surfaces for different washing times. Error bars represent standard deviations.

Figure 13: Fluorescence micrographs of the bulk material B (A, C, E, G) and the best bacteria repelling condition S1(B-D-F-H) for 15, 30, 60 and 120 min, respectively.

Tables

Table 1: Main specifications of the employed laser system.

Wavelength	λ	1,064 nm
Max average power	P_{avg}	50 W
Pulse repetition rate	PRR	20-80 kHz
Max pulse energy	E_{max}	1 mJ
Pulse duration	τ_{on}	250 ns
Beam quality	M^2	1.7
Collimated beam diameter	d_c	5.9 mm
Focusing lens	f	100 mm
Focused beam diameter	d_0	39 μm

Table 2: Experimental plan for LμP treatments.

Fixed parameters		Levels
Pulse repetition rate	PRR [kHz]	65
Pitch	p [μm]	10
Defocusing	Δz [mm]	2
Gas type		N_2
Gas pressure	[bar]	0.3

Varied parameters		Levels
Laser energy	E [mJ]	0.19, 0.28, 0.38, 0.47
Scanning speed	v [m/min]	12, 24, 48, 96, 192
Number of passes	N	1, 2, 4

Measured variables	
Surface roughness	Sa,r [nm]
Surface waviness	Sa,w [nm]
Surface wettability	Contact angle [°]

Table 3: Experimental plan for the first phase bacteria adhesion tests.

Fixed parameters	Levels
Starting bacteria concentration	10-20 cells/mm^2
Incubation time	2 hrs
Washing solution	0.5 M NaCl + 0.1% Triton
Washing time	1 hr

Varied parameters	Levels
Substrate type	B, S1, S2

Table 4: Experimental plan for the second phase in bacteria adhesion tests.

Fixed parameters	Levels
Starting bacteria concentration	10-20 cells/mm^2
Incubation time	2 hrs
Washing solution	0.5 M NaCl + 0.1% Triton

Varied parameters	Levels
Substrate type	B, S1
Washing time	15, 30, 60 and 120 mins

Table 5: Regression models and summary, where Sa,r and Sa,w are expressed in nm, E in mJ and v in m/min.

Model	R^2_{adj}
$Sa,r = 336.0\,E - 6.86 \cdot 10^{-2}\,v - 344.7\,E^2 + 1.163 \cdot 10^{-3}\,v^2 - 0.720\,E\,v$	99%
$1/\sqrt{Sa,w} = -0.1655 + 0.2316\,E - 2.5 \cdot 10^{-4}\,v - 7.00 \cdot 10^{-3}\,E^2 + 2 \cdot 10^{-6}\,v^2 - 1.081 \cdot 10^{-3}\,E\,v$	80%